

Magnetic order without tetragonal symmetry-breaking in iron arsenides: microscopic mechanism and spin-wave spectrum

Xiaoyu Wang, Jian Kang, and Rafael M. Fernandes

School of Physics and Astronomy, University of Minnesota, Minneapolis 55455, USA

Most iron-based superconductors undergo a transition to a magnetically ordered state characterized by staggered stripes of parallel spins. With ordering vectors $(\pi, 0)$ or $(0, \pi)$, this magnetic state breaks the high-temperature tetragonal symmetry of the system, which is manifested by a splitting of the lattice Bragg peaks. Remarkably, recent experiments in hole-doped iron arsenides reported an ordered state that displays magnetic Bragg peaks at $(\pi, 0)$ and $(0, \pi)$ but remains tetragonal. Despite being inconsistent with a magnetic stripe configuration, this unusual magnetic phase can be described in terms of a double- \mathbf{Q} magnetic structure consisting of an equal-weight superposition of the ordering vectors $(\pi, 0)$ and $(0, \pi)$. Here we show that a non-collinear double- \mathbf{Q} magnetic configuration, dubbed *orthomagnetic*, arises naturally within an itinerant three-band microscopic model for the iron pnictides. In particular, we find that strong deviations from perfect nesting and residual interactions between the electron pockets favor the orthomagnetic over the stripe magnetic state. Using an effective low-energy model, we also calculate the spin-wave spectrum of the orthomagnetic state. In contrast to the stripe state, there are three Goldstone modes, manifested in all diagonal and one off-diagonal component of the spin-spin correlation function. The total magnetic structure factor displays two anisotropic spin-wave branches emerging from both $(\pi, 0)$ and $(0, \pi)$ momenta, in contrast to the case of domains of stripe order, where only one spin-wave branch emerges from each momentum. We propose that these unique features of the orthomagnetic state can be used to unambiguously distinguish it from the stripe state via neutron scattering experiments, and discuss the implications of its existence to the nature of the magnetism of the iron arsenides.

I. INTRODUCTION

Unveiling the nature of the magnetic state of the iron-based materials [1] is imperative to advance our understanding of their superconducting state. Indeed, the vast majority of iron arsenide parent compounds display a stripe magnetically ordered state, characterized by spins arranged parallel to each other along one in-plane direction (either the \hat{x} or the \hat{y} axis) and anti-parallel to each other along the other direction, see Fig. 1a-b (for reviews, see [2]). Its main manifestation is the presence of magnetic Bragg peaks at the momenta $\mathbf{Q}_1 = (\pi, 0)$ or $\mathbf{Q}_2 = (0, \pi)$ (in the Fe-square lattice), which correspond to the ordering vectors of the two possible stripe states. Because the samples form twin domains, both magnetic peaks are observed in the same material by neutron scattering experiments [3].

Since the stripe state breaks the tetragonal C_4 point-group symmetry of the system down to the orthorhombic C_2 symmetry, a splitting of the lattice Bragg peaks is also observed by x-ray scattering [4]. Remarkably, this orthorhombic distortion is observed in many systems at a temperature T_s above the onset of long-range magnetic order at T_N . As a result, an intense debate has been taking place in the community about the origin of the magnetism in these materials [5–9]. One scenario proposes that the magnetic transition is triggered only because ferro-orbital order sets in at $T_s > T_N$, effectively renormalizing the exchange couplings between neighboring Fe atoms and enabling magnetic order to be stabilized [10–12]. A different scenario proposes that the structural transition at T_s is a manifestation of an emergent Ising-nematic phase driven by magnetic fluctuations present

near T_N [13–16].

Recently, new experiments have provided important clues for this hotly debated topic. In particular, neutron and x-ray scattering measurements in $\text{Ba}(\text{Fe}_{1-x}\text{Mn}_x)_2\text{As}_2$ [17] and $(\text{Ba}_{1-x}\text{Na}_x)\text{Fe}_2\text{As}_2$ [18] reported a regime in which the system displays magnetic Bragg peaks at \mathbf{Q}_1 and \mathbf{Q}_2 but no splitting of the lattice Bragg peaks. In $(\text{Ba}_{1-x}\text{K}_x)\text{Fe}_2\text{As}_2$, recent thermal expansion measurements observed no orthorhombic distortion inside the magnetically ordered state near optimal doping [19]. Interestingly, in $(\text{Ba}_{1-x}\text{K}_x)\text{Fe}_2\text{As}_2$ under pressure, an unidentified ordered state was also observed inside the magnetic phase [20], which could be connected to the C_4 -magnetic state found in $(\text{Ba}_{1-x}\text{K}_x)\text{Fe}_2\text{As}_2$ at ambient pressure. The only magnetic states compatible with these reports are double- \mathbf{Q} structures corresponding to a C_4 -preserving linear combination of the two possible magnetic order parameters [21–24]. Domains of the two different stripe states are incompatible with these observations, since they would cause a four-fold splitting of the lattice Bragg peaks [4]. More specifically, writing the spin at position \mathbf{r} as $\mathbf{S}(\mathbf{r}) = \mathbf{M}_1 e^{i\mathbf{Q}_1 \cdot \mathbf{r}} + \mathbf{M}_2 e^{i\mathbf{Q}_2 \cdot \mathbf{r}}$, the experimental observations of tetragonal magnetic ground states in $\text{Ba}(\text{Fe}_{1-x}\text{Mn}_x)_2\text{As}_2$, $(\text{Ba}_{1-x}\text{K}_x)\text{Fe}_2\text{As}_2$, and $(\text{Ba}_{1-x}\text{Na}_x)\text{Fe}_2\text{As}_2$ imply a phase with $|\mathbf{M}_1| = |\mathbf{M}_2|$. If $\mathbf{M}_1 \perp \mathbf{M}_2$, one obtains a non-collinear phase dubbed orthomagnetic [23] (see Fig. 1c), whereas if $\mathbf{M}_1 \parallel \mathbf{M}_2$, a non-uniform phase emerges where half of the sites are non-magnetic (see Fig. 1d) [22]. In both cases, the system breaks translational symmetry but not the C_4 point-group symmetry. The possible existence of multi- \mathbf{Q} magnetic structures is not a particular feature of the iron arsenides, as it has also been proposed in a variety

of systems, such as the Kondo system CeAl_2 [25, 26], the borocarbide $\text{GdNi}_2\text{B}_2\text{C}$ [27, 28], the rocksalt-structure uranium pnictide USb [29], and even γ -Mn alloys [30].

Taken at face value, the experimental findings of C_4 -preserving magnetic order in the iron arsenides imply that magnetism can exist even in the absence of ferro-orbital order, providing indirect evidence for a magnetic mechanism for the structural transition in the compounds that display stripe magnetism [18]. Furthermore, because the non-collinear and non-uniform states are not present in the ground state manifold of the local-spin J_1 - J_2 model [31], their existence favors an itinerant low-energy model for the magnetic properties of the iron superconductors [7]. Therefore, firmly establishing experimentally the existence of these tetragonal magnetic phases will have a strong impact in our understanding of these materials. So far, the main evidence in favor of their existence is the absence of orthorhombic distortion concomitant with the appearance of magnetic Bragg peaks at \mathbf{Q}_1 and \mathbf{Q}_2 . However, because of the resolution limitations intrinsic to x-ray or thermal expansion measurements [32, 33], it is desirable to search for other unambiguous experimental signatures of these phases. While previous works have focused on the signatures of the non-uniform double- \mathbf{Q} phase [21], the properties of the orthomagnetic state remain largely unexplored.

In this paper, we show explicitly from a microscopic three-band model that strong deviations from particle-hole symmetry (perfect nesting) favor a tetragonal magnetic state over the stripe state. Interestingly, the orthomagnetic state is selected by a residual electronic interaction that does not participate explicitly in the formation of the magnetic state [22]. These theoretical results are complementary to those reported in Ref. [18], which found that deep inside the stripe ordered state a second instability towards a tetragonal magnetic state emerges.

Using an effective low-energy model for the orthomagnetic state, we also calculate its spin-wave spectrum. In contrast to the stripe state, which displays a doubly-degenerate Goldstone mode, we find three Goldstone modes that give rise to two distinct spin-wave branches emerging from both \mathbf{Q}_1 and \mathbf{Q}_2 . Furthermore, the three diagonal components of the spin-spin correlation function \mathcal{S}_{xx} , \mathcal{S}_{yy} , \mathcal{S}_{zz} , and the off-diagonal \mathcal{S}_{xz} term, display spin-wave modes at low energies, implying that in all directions the excitations behave as gapless longitudinal-like modes, as expected for a non-collinear configuration that breaks all spin-space rotational symmetries. We argue that these signatures of the low-energy spin spectrum of the orthomagnetic state can be unambiguously distinguished from those arising from domains of stripe magnetic states in both unpolarized and polarized neutron scattering measurements. Thus, our studies provide concrete criteria to establish the existence of the orthomagnetic state beyond the indirect evidence of an absent orthorhombic distortion.

Our paper is organized as follows: in Section II, we review the microscopic model for the magnetic instability

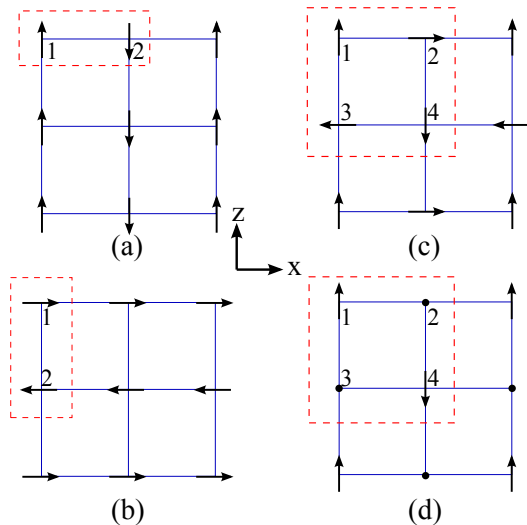


Figure 1: Magnetic ground state configurations for (a) $\mathbf{Q}_1 = (\pi, 0)$ stripe order (b) $\mathbf{Q}_2 = (0, \pi)$ stripe order (c) double- \mathbf{Q} non-collinear (orthomagnetic) order and (d) double- \mathbf{Q} non-uniform magnetic order. The dashed rectangle labels the magnetic unit cell in each case. While (a) and (b) are orthorhombic, (c) and (d) are tetragonal.

proposed in Refs. [15, 22] and extend the analysis by including the effects of the residual electronic interactions and by computing the Ginzburg-Landau coefficients in the regime far from perfect nesting. In Section III we present an effective low-energy model for the orthomagnetic state whose spin-wave dispersions can be appropriately treated within the Holstein-Primakoff formalism. We calculate both the spin-wave modes and the components of the spin-spin correlation function, contrasting to the stripe magnetic case. Section IV is devoted to the concluding remarks and to the applicability of our results to other materials that may display orthomagnetic order, such as the heavy-fermion related compound GdRhIn_5 [34].

II. MICROSCOPIC MECHANISM FOR THE ORTHOMAGNETIC ORDER

We start with the itinerant three-band model that was previously used to explain the magnetic properties of the iron arsenides near perfect nesting [15, 22]. The non-interacting part consists of:

$$H_0 = \sum_{\mathbf{k}a\alpha} \varepsilon_{a,\mathbf{k}} c_{a,\mathbf{k}\alpha}^\dagger c_{a,\mathbf{k}\alpha} \quad (1)$$

where α is the spin index, \mathbf{k} is the momentum, and $a = h, e_1, e_2$ refer to, respectively, the central hole pocket and the electron pockets centered at $\mathbf{Q}_1 = (\pi, 0)$ and $\mathbf{Q}_2 = (0, \pi)$. The band dispersions near the Fermi level can be conveniently parametrized as:

$$\begin{aligned}
\varepsilon_{h,\mathbf{k}} &= -\varepsilon_{\mathbf{k}} \\
\varepsilon_{e_1,\mathbf{k}+\mathbf{Q}_1} &= \varepsilon_{\mathbf{k}} - (\delta_\mu + \delta_m \cos 2\theta) \\
\varepsilon_{e_2,\mathbf{k}+\mathbf{Q}_2} &= \varepsilon_{\mathbf{k}} - (\delta_\mu - \delta_m \cos 2\theta)
\end{aligned} \tag{2}$$

where $\varepsilon_{\mathbf{k}} = \frac{k^2}{2m} - \varepsilon_0$ is a parabolic-like band dispersion, θ is the angle around the electron pocket, δ_m describes the ellipticity of the electron pockets, and δ_μ is proportional to changes in the carrier concentration (doping). Note that for $\delta_m = \delta_\mu = 0$, the system has perfect particle-hole symmetry and the hole and electron pockets are perfectly nested.

Following Ref. [35, 36], there are eight types of interactions connecting the three Fermi pockets, corresponding to density-density (U_1, U_4, U_5, U_6), spin-exchange (U_2, U_7) and pair-hopping (U_3, U_8) interactions respectively. The interaction Hamiltonian is:

$$\begin{aligned}
H_{\text{int}} &= U_1 \sum c_{h\alpha}^\dagger c_{e_1\beta}^\dagger c_{e_1\beta} c_{h\alpha} + U_2 \sum c_{h\alpha}^\dagger c_{e_1\beta}^\dagger c_{h\beta} c_{e_1\alpha} \\
&+ \frac{U_3}{2} \sum (c_{h\alpha}^\dagger c_{h\beta}^\dagger c_{e_1\beta} c_{e_1\alpha} + \text{h.c.}) \\
&+ \frac{U_4}{2} \sum c_{e_1\alpha}^\dagger c_{e_1\beta}^\dagger c_{e_1\beta} c_{e_1\alpha} + \frac{U_5}{2} \sum c_{h\alpha}^\dagger c_{h\beta}^\dagger c_{h\beta} c_{h\alpha} \\
&+ U_6 \sum c_{e_1\alpha}^\dagger c_{e_2\beta}^\dagger c_{e_2\beta} c_{e_1\alpha} + U_7 \sum c_{e_1\alpha}^\dagger c_{e_2\beta}^\dagger c_{e_1\beta} c_{e_2\alpha} \\
&+ \frac{U_8}{2} \sum (c_{e_1\alpha}^\dagger c_{e_1\beta}^\dagger c_{e_2\beta} c_{e_2\alpha} + \text{h.c.})
\end{aligned} \tag{3}$$

For simplicity of notation, the momentum indices are all suppressed with the implicit constraint of momentum conservation. To study the instability towards magnetic order, we project all the interactions in the spin-density wave (SDW) channel – which is the leading one, according to RG and fRG calculations [36, 37]. The only interactions that contribute directly to the SDW instability are U_1 and U_3 . The partition function, restricted to this channel only, can then be written in the functional field form:

$$\mathcal{Z} = \int \mathcal{D}c^\dagger \mathcal{D}c \exp(-S) \tag{4}$$

with the action :

$$S = \int_0^\beta d\tau \sum_{i\mathbf{k}\sigma} c_{i\mathbf{k}\sigma}^\dagger \partial_\tau c_{i\mathbf{k}\sigma} + H_0 + H_{\text{SDW}} \tag{5}$$

and the SDW-decoupled interaction:

$$H_{\text{SDW}} = -I \sum_{i\mathbf{k}\mathbf{k}'\mathbf{q}} \left(c_{h\mathbf{k}\alpha}^\dagger \sigma_{\alpha\beta} c_{e_i\mathbf{k}+\mathbf{q}\beta} \right) \cdot \left(c_{e_i\mathbf{k}'\gamma}^\dagger \sigma_{\gamma\delta} c_{h\mathbf{k}'-\mathbf{q}\delta} \right) \tag{6}$$

where $I = U_1 + U_3$. We now introduce the Hubbard-Stratonovich fields \mathbf{M}_i , which are proportional to the staggered magnetization with ordering vector \mathbf{Q}_i , i.e. $\langle \mathbf{M}_i \rangle = I \sum_{\mathbf{k}} \langle c_{h\mathbf{k}\alpha}^\dagger \sigma_{\alpha\beta} c_{e_i\mathbf{k}+\mathbf{q}\beta} \rangle$, via $\exp(-H_{\text{SDW}}) \propto \int \mathcal{D}\mathbf{M}_i \exp(-S_{\text{SDW}}[\mathbf{M}_i])$ with:

$$\begin{aligned}
S_{\text{SDW}}[\mathbf{M}_i] &= \sum_{i\mathbf{q}} \frac{\mathbf{M}_{i\mathbf{q}} \cdot \mathbf{M}_{i-\mathbf{q}}}{I} \\
&- \sum_{i\mathbf{q}\mathbf{k}} \left(\mathbf{M}_{i\mathbf{q}} \cdot c_{e_i\mathbf{k}\gamma}^\dagger \sigma_{\gamma\delta} c_{h\mathbf{k}-\mathbf{q}\delta} + \text{h.c.} \right)
\end{aligned} \tag{7}$$

Following Ref. [15], we then integrate out the electronic degrees of freedom, obtaining an effective action for the magnetic degrees of freedom:

$$\begin{aligned}
\mathcal{Z} &= \int \mathcal{D}c^\dagger \mathcal{D}c \mathcal{D}\mathbf{M}_i \exp(-S[c^\dagger, \mathbf{M}_i]) \\
&= \int \mathcal{D}\mathbf{M}_i \exp(-S_{\text{eff}}[\mathbf{M}_i])
\end{aligned} \tag{8}$$

For a finite-temperature magnetic transition, $S_{\text{eff}}[\mathbf{M}_i] = F[\mathbf{M}_i]/T$, where $F[\mathbf{M}_i]$ is the free energy functional. Near the magnetic transition, we can expand the functional in powers of the magnetic order parameters, deriving the Ginzburg-Landau expansion:

$$\begin{aligned}
F[\mathbf{M}_i] &= \frac{a}{2} (\mathbf{M}_1^2 + \mathbf{M}_2^2) + \frac{u}{4} (\mathbf{M}_1^2 + \mathbf{M}_2^2)^2 \\
&- \frac{g}{4} (\mathbf{M}_1^2 - \mathbf{M}_2^2)^2 + w (\mathbf{M}_1 \cdot \mathbf{M}_2)^2
\end{aligned} \tag{9}$$

In the vicinity of the magnetic transition, $a \approx N_f(T - T_c)$, where N_f is the density of states at the Fermi surface. The coefficients u, g , and w are given by [15]:

$$\begin{aligned}
u &= A + B \\
g &= B - A \\
w &= 0
\end{aligned} \tag{10}$$

with:

$$\begin{aligned}
A &= \int_k G_{h,\mathbf{k}}^2 G_{e_1,\mathbf{k}+\mathbf{Q}_1}^2 \\
&= \int_k \left(\frac{1}{i\omega_n + \varepsilon_{\mathbf{k}}} \right)^2 \left(\frac{1}{i\omega_n - \varepsilon_{\mathbf{k}} + \delta_\mu + \delta_m \cos 2\theta} \right)^2, \\
B &= \int_k G_{h,\mathbf{k}}^2 G_{e_1,\mathbf{k}+\mathbf{Q}_1} G_{e_2,\mathbf{k}+\mathbf{Q}_2} \\
&= \int_k \left(\frac{1}{i\omega_n + \varepsilon_{\mathbf{k}}} \right)^2 \frac{1}{i\omega_n - \varepsilon_{\mathbf{k}} + \delta_\mu + \delta_m \cos 2\theta} \\
&\quad \times \frac{1}{i\omega_n - \varepsilon_{\mathbf{k}} + \delta_\mu - \delta_m \cos 2\theta},
\end{aligned} \tag{11}$$

Here, $G_{a,\mathbf{k}}$ is the non-interacting fermionic Green's function for pocket a , $G_{a,\mathbf{k}}^{-1} = i\omega_n - \varepsilon_{a,\mathbf{k}}$, and $\int_k \rightarrow \sum_n \int \frac{d\mathbf{k}}{(2\pi)^d}$, with Matsubara frequency $\omega_n = (2n+1)\pi T$. After integrating out the momentum, we obtain:

$$A = N_f T \pi \sum_{n=0}^{\infty} \text{Im} \int_{\theta} \frac{1}{\left(i\omega_n + \frac{\delta_{\mu}}{2} + \frac{\delta_m}{2} \cos 2\theta\right)^3}$$

$$B = N_f T \pi \sum_{n=0}^{\infty} \text{Im} \int_{\theta} \frac{i\omega_n + \frac{\delta_{\mu}}{2}}{\left(\left(i\omega_n + \frac{\delta_{\mu}}{2}\right)^2 - \left(\frac{\delta_m}{2} \cos 2\theta\right)^2\right)^2} \quad (12)$$

with $\int_{\theta} = \int_0^{2\pi} \frac{d\theta}{2\pi}$. A straightforward minimization of Eq. (9) reveals that the stripe magnetic state is the global free energy minimum for $g > \max(0, -w)$, whereas a tetragonal magnetic state is the lowest energy ground state for $g < \min(0, -w)$. Since in the model above $w = 0$, the sign of g determines uniquely the symmetry of the magnetic ground state. Note that the free energy functional is bounded for $u > \max(g, 0, -w)$.

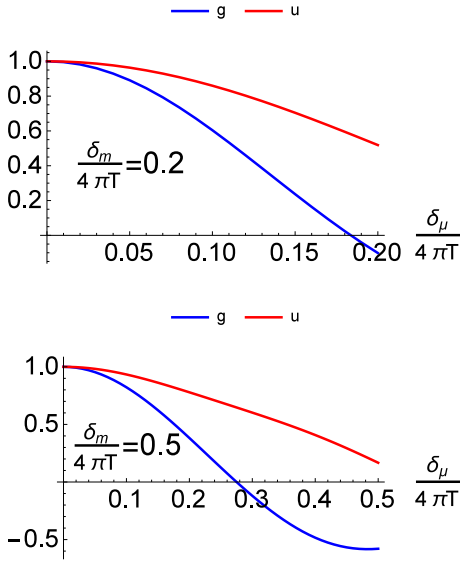


Figure 2: Quartic Ginzburg-Landau coefficients u (red) and g (blue) of the free energy (9) as function of $\delta_{\mu}/(4\pi T)$ for $\delta_m/(4\pi T) = 0.2$ (left) and $\delta_m/(4\pi T) = 0.5$ (right). Note that u and g are normalized by their values at $\delta_{\mu} = 0$. For $g > 0$, the magnetic ground state is the stripe state, which lowers the tetragonal symmetry to orthorhombic. For $g < 0$, tetragonal symmetry is preserved, and either a non-collinear or a non-uniform double- \mathbf{Q} magnetic state arises. Notice that the free energy remains bounded as long as $u > 0$.

The previous analysis of the Ginzburg-Landau coefficients (12) in Ref. [15] focused on the regime near perfect nesting, where $\delta_{\mu}, \delta_m \ll T$. In this case, $g \propto \delta_m^2 > 0$ and the ground state is the stripe magnetic one. Here, we extend the analysis beyond small deviations from perfect nesting by numerically computing Eqs. (12) for arbitrary δ_{μ}/T , δ_m/T (the constraint $\delta_m \geq \delta_{\mu}$ is imposed to ensure that hot spots are present, as seen experimentally). To mimic the phase diagrams of $\text{Ba}(\text{Fe}_{1-x}\text{Mn}_x)_2\text{As}_2$,

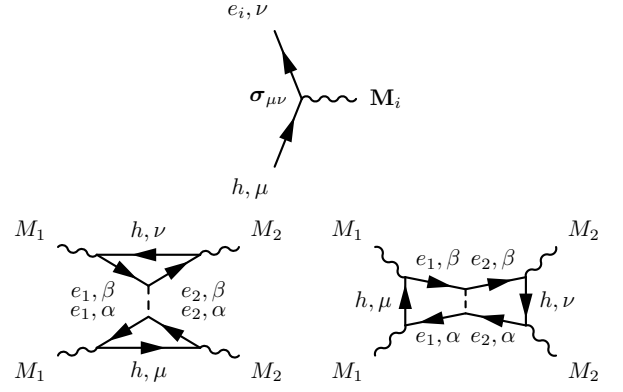


Figure 3: Top panel: The vertex that couples the magnetic order parameter to the low-energy fermionic states, which has a $\mathbf{M}_i \cdot \boldsymbol{\sigma}$ structure. Solid lines refer to the non-interacting electronic Green's functions. Bottom panel: the Feynman diagrams containing the leading-order corrections to the free energy arising from the residual U_7 interaction.

($\text{Ba}_{1-x}\text{K}_x$) Fe_2As_2 , and ($\text{Ba}_{1-x}\text{Na}_x$) Fe_2As_2 , we change the parameter δ_{μ} (proportional to the carrier concentration) for a fixed value of the ellipticity δ_m . Fig 2 shows the results for $\delta_m/T = 0.8\pi$ and $\delta_m/T = 2\pi$. For small values of δ_{μ} , both u and g are positive, and the stripe magnetic state is favored. However, as δ_{μ} becomes larger, regardless of the value of δ_m , g becomes negative, indicating that the magnetic ground state becomes a double- \mathbf{Q} tetragonal phase. Since u remains positive when g first changes sign, the free energy remains bounded, i.e. the mean-field transition is second-order. These results are in qualitative agreement with the phase diagrams of $\text{Ba}(\text{Fe}_{1-x}\text{Mn}_x)_2\text{As}_2$, ($\text{Ba}_{1-x}\text{K}_x$) Fe_2As_2 , and ($\text{Ba}_{1-x}\text{Na}_x$) Fe_2As_2 , which display the tetragonal magnetic phase only for sufficiently strong doping concentration. We note that a tetragonal magnetic state was also reported in other itinerant approaches for the iron pnictides [22–24], as well as in a strong-coupling two-orbital ladder model [38].

Because $w = 0$ in our model, when g becomes negative the system does not distinguish between the two possible tetragonal magnetic states, namely, the orthomagnetic one ($w > 0$, $\mathbf{M}_1 \perp \mathbf{M}_2$) and the non-uniform one ($w < 0$, $\mathbf{M}_1 \parallel \mathbf{M}_2$). Although the terms arising purely from the band structure do not contribute to the w coefficient, the residual interactions in Eq. (3) that do not participate in the SDW instability (namely U_2, U_4, U_5, U_6, U_7 , and U_8) give rise to such a term, as pointed out in Ref. [22]. Computing the contributions of the residual interactions to the free energy, we obtain:

$$\tilde{F}[\mathbf{M}_i] = \frac{1}{4} (-\tilde{u}_2 + \tilde{u}_4 + \tilde{u}_5 + \tilde{u}_6 - \tilde{u}_7 + \tilde{u}_8) (\mathbf{M}_1^2 + \mathbf{M}_2^2)^2$$

$$- \frac{1}{4} (-\tilde{g}_4 + \tilde{g}_6 - \tilde{g}_7 + \tilde{g}_8) (\mathbf{M}_1^2 - \mathbf{M}_2^2)^2$$

$$+ \tilde{w}_7 (\mathbf{M}_1 \cdot \mathbf{M}_2)^2 \quad (13)$$

The Ginzburg-Landau coefficients can be obtained in a straightforward way using diagrammatics. In Fig. 3 we show the two diagrams arising from the U_7 interaction, which contribute to \tilde{u}_7 , \tilde{g}_7 , and \tilde{w}_7 . Additional computational details are discussed in Appendix A. The coefficients of the quartic symmetric term are given by:

$$\begin{aligned}
\tilde{u}_2 &= 8U_2 \left(\int_k G_{h,\mathbf{k}} G_{e_1,\mathbf{k}+\mathbf{Q}_1}^2 \right) \left(\int_k G_{h,\mathbf{k}}^2 G_{e_1,\mathbf{k}+\mathbf{Q}_1} \right) \\
\tilde{u}_4 &= 2U_4 \left(\int_k G_{h,\mathbf{k}} G_{e_1,\mathbf{k}+\mathbf{Q}_1}^2 \right)^2 \\
\tilde{u}_5 &= 4U_5 \left(\int_k G_{h,\mathbf{k}}^2 G_{e_1,\mathbf{k}+\mathbf{Q}_1} \right)^2 \\
\tilde{u}_6 &= 2U_6 \left[2 \left(\int_k G_{h,\mathbf{k}} G_{e_1,\mathbf{k}+\mathbf{Q}_1}^2 \right)^2 \right. \\
&\quad \left. - \left(\int_k G_{h,\mathbf{k}} G_{e_1,\mathbf{k}+\mathbf{Q}_1} G_{e_2,\mathbf{k}+\mathbf{Q}_2} \right)^2 \right] \\
\tilde{u}_7 &= 2U_7 \left(\int_k G_{h,\mathbf{k}} G_{e_1,\mathbf{k}+\mathbf{Q}_1}^2 \right)^2 \\
\tilde{u}_8 &= 2U_8 \left(\int_k G_{h,\mathbf{k}} G_{e_1,\mathbf{k}+\mathbf{Q}_1} G_{e_2,\mathbf{k}+\mathbf{Q}_2} \right)^2 \quad (14)
\end{aligned}$$

whereas the coefficients of the quartic anti-symmetric term read:

$$\begin{aligned}
\tilde{g}_4 &= 2U_4 \left(\int_k G_{h,\mathbf{k}} G_{e_1,\mathbf{k}+\mathbf{Q}_1}^2 \right)^2 \\
\tilde{g}_6 &= 2U_6 \left[2 \left(\int_k G_{h,\mathbf{k}} G_{e_1,\mathbf{k}+\mathbf{Q}_1}^2 \right)^2 \right. \\
&\quad \left. - \left(\int_k G_{h,\mathbf{k}} G_{e_1,\mathbf{k}+\mathbf{Q}_1} G_{e_2,\mathbf{k}+\mathbf{Q}_2} \right)^2 \right] \\
\tilde{g}_7 &= 2U_7 \left(\int_k G_{h,\mathbf{k}} G_{e_1,\mathbf{k}+\mathbf{Q}_1}^2 \right)^2 \\
\tilde{g}_8 &= 2U_8 \left(\int_k G_{h,\mathbf{k}} G_{e_1,\mathbf{k}+\mathbf{Q}_1} G_{e_2,\mathbf{k}+\mathbf{Q}_2} \right)^2 \quad (15)
\end{aligned}$$

and the coefficient of the quartic scalar-product term yields:

$$\tilde{w}_7 = 4U_7 \left(\int_k G_{h,\mathbf{k}} G_{e_1,\mathbf{k}+\mathbf{Q}_1} G_{e_2,\mathbf{k}+\mathbf{Q}_2} \right)^2 \quad (16)$$

At perfect nesting, an overall factor proportional to the Green's functions product $\left(\int_k G_{h,\mathbf{k}}^2 G_{e_1,\mathbf{k}+\mathbf{Q}_1} \right)^2$ appears in all terms. In this limit, our results become identical to those found in Ref. [22], which computed the corrections to the magnetic ground state energy in the ordered state using a sequence of Bogoliubov transformations. In

the paramagnetic state, however, which is our case of interest, this Green's functions product vanishes – as also pointed out in Ref. [22]. The corrections due to the residual interactions naturally become non-zero – and in fact positive – once one considers small deviations from perfect nesting. For \tilde{w}_7 , we find:

$$\tilde{w}_7 \approx 4U_7 \left(\frac{7\zeta(3)N_f\delta_\mu}{8\pi^2T^2} \right)^2 \quad (17)$$

Because the band dispersions do not contribute to the term $(\mathbf{M}_1 \cdot \mathbf{M}_2)^2$, the fact that $\tilde{w}_7 > 0$ is very important, as it implies that the residual interaction U_7 selects the orthomagnetic state over the non-uniform state (assuming that $U_7 > 0$, as one would expect). Therefore, when $g_{\text{eff}} = g + \tilde{g}$ changes sign, the system tends to form the non-collinear tetragonal magnetic state shown in Fig. 1c. In the next section, we will discuss the magnetic spectrum of such a state. Before proceeding, we emphasize that, as pointed out by two of us in a previous communication [21], other mechanisms may favor a different sign for the w coefficient – such as the coupling to soft Neel-like magnetic fluctuations – which could stabilize the non-uniform tetragonal magnetic state shown in Fig. 1d.

III. SPIN-WAVE SPECTRUM

Having established the conditions under which the orthomagnetic state becomes the ground state of the system, we now discuss its experimental manifestations. The most evident one is the lack of tetragonal symmetry breaking, since the orthomagnetic order has an equal weight of the order parameters \mathbf{M}_1 and \mathbf{M}_2 associated with the ordering vectors $\mathbf{Q}_1 = (\pi, 0)$ and $\mathbf{Q}_2 = (0, \pi)$, respectively. The preservation of C_4 symmetry can in principle be detected by x-ray or neutron scattering via the absence of splitting of the lattice Bragg peaks across the magnetic transition. However, given the resolution limitations of scattering measurements, it is desirable to consider other properties that identify unambiguously the orthomagnetic state.

In this section, we study in details the spin-wave spectrum of the orthomagnetic phase, comparing it to the stripe phase. As we are interested in the low-energy behavior, there are two alternative approaches to compute the spin-wave spectrum: the first is by evaluating self-consistently the poles of the spin-spin correlation function deep inside the magnetically ordered state within the itinerant approach described in the previous section [39]. The second alternative is to build a phenomenological localized-spin model that gives the same ground states as the itinerant model, and then use Holstein-Primakoff (HP) bosons to compute the spin-wave dispersion. Given the simplicity of the latter, we here consider a Heisenberg model on a two-dimensional square lattice, with nearest-

neighbor and next-nearest neighbor interactions:

$$H = J_1 \sum_{\langle i,j \rangle} \mathbf{S}_i \cdot \mathbf{S}_j + J_2 \sum_{\langle\langle i,j \rangle\rangle} \mathbf{S}_i \cdot \mathbf{S}_j - \frac{K}{S^2} \sum_{\langle i,j \rangle} (\mathbf{S}_i \cdot \mathbf{S}_j)^2 \quad (18)$$

where $\langle \dots \rangle$ and $\langle\langle \dots \rangle\rangle$ denote nearest-neighbors and next-nearest neighbors, and $J_1 > 0$, $J_2 > J_1/2$ are the respective antiferromagnetic exchange interactions. The biquadratic term K selects between the stripe phase ($K > 0$) and the orthomagnetic phase ($K < 0$) in the classical regime. We emphasize that this is a phenomenological model constructed to describe the ground states obtained in Section II. Indeed, if it was the classical J_1 - J_2 model, K would be restricted to small positive values only [31]. Instead, here K should be understood as a phenomenological parameter, analogous to the parameter g calculated in Eq. (9). In fact, a Ginzburg-Landau expansion of this toy Heisenberg model would result in a free energy equivalent to that of Eq. (9), evidencing the fact that both models share the same low-energy properties [40]. Therefore, the use of this localized-spin model should be understood simply as a tool to evaluate the spin-wave spectrum, and not an implication that local moments are necessarily present in the system. Incidentally, we note that other Heisenberg models with ring exchange interactions can also display orthomagnetic order [41].

We emphasize that a strict two-dimensional model does not have long-range Heisenberg magnetic order, according to Mermin-Wagner theorem. As a result, we assume here that the system is formed by weakly-coupled layers. Such a small inter-layer coupling can nevertheless be neglected in what regards the main properties of the spin-wave dispersions. To obtain the spin-wave spectrum of the Hamiltonian (18), we follow Refs. [42, 43] and introduce locally HP bosons for each of the r spins in a single magnetic unit cell:

$$\begin{aligned} \mathbf{S}_z^{(r)} &= S - a^{(r)\dagger} a^{(r)} \\ \mathbf{S}_+^{(r)} &= \sqrt{2S - a^{(r)\dagger} a^{(r)}} a^{(r)} \\ \mathbf{S}_-^{(r)} &= a^{(r)\dagger} \sqrt{2S - a^{(r)\dagger} a^{(r)}} \end{aligned} \quad (19)$$

Note that the spin coordinate system is defined locally, such that the local spin is always parallel to the local $+\hat{\mathbf{z}}$ axis. For convenience, the two-dimensional lattice plane xy is chosen to be the xz spin-plane, as shown in Fig. 1. Since different types of spins within a magnetic unit cell have their own degree of freedom, the number of HP bosons (labeled by r) is equal to the number of spins within a magnetic unit cell. Thus, the stripe state has $r = 1, 2$ whereas the orthomagnetic state has $r = 1, 2, 3, 4$, as labeled in Fig. 1. The Fourier transform of the HP bosons is defined as

$$a_{\mathbf{k}}^{(r)} = \sum_{i \in r} a_i^{(r)} e^{-i\mathbf{k} \cdot \mathbf{x}_i^{(r)}} \quad (20)$$

where i labels different magnetic unit cells, and $\mathbf{x}_i^{(r)}$ is the position of the r -th spin in the i -th magnetic unit

cell. For convenience, we define:

$$\Psi_{\mathbf{k}}^\dagger \equiv \left(a_{\mathbf{k}}^{(1)\dagger}, a_{-\mathbf{k}}^{(1)}, a_{\mathbf{k}}^{(2)\dagger}, a_{-\mathbf{k}}^{(2)}, \dots \right) \quad (21)$$

Because we are interested in the classical limit, we perform a large S expansion and keep only terms that are quadratic in the bosonic operators. In this case, the Heisenberg Hamiltonian can be re-expressed as:

$$H = H_0 + \frac{1}{2} \sum_{\mathbf{k}} \Psi_{\mathbf{k}}^\dagger \hat{\mathcal{H}}_{\mathbf{k}} \Psi_{\mathbf{k}} \quad (22)$$

where H_0 is the classical ground state energy for a given spin configuration. The spin-wave modes can be obtained by a generalized Bogoliubov transformation, $\Psi_{\mathbf{k}} = \hat{\mathcal{U}}_{\mathbf{k}} \Phi_{\mathbf{k}}$. To ensure that the transformed operators satisfy the correct bosonic commutation relations, it is convenient to introduce the Bogoliubov metric:

$$\hat{\eta} = \text{diag}(1, -1, 1, -1, \dots) \quad (23)$$

Then, the generalized Bogoliubov transformation satisfies:

$$\begin{aligned} \hat{\mathcal{U}}_{\mathbf{k}}^\dagger \hat{\eta} \hat{\mathcal{U}}_{\mathbf{k}} &= \hat{\eta} \\ \hat{\mathcal{U}}_{\mathbf{k}}^{-1} \left(\hat{\eta} \hat{\mathcal{H}}_{\mathbf{k}} \right) \hat{\mathcal{U}}_{\mathbf{k}} &= \left(\hat{\eta} \hat{\mathcal{H}}_{\mathbf{k}} \right)^{\text{diag}} \end{aligned} \quad (24)$$

The spin-wave modes are therefore the eigenvalues of $\hat{\eta} \hat{\mathcal{H}}_{\mathbf{k}}$.

A. Stripe phase: spin-wave modes

As discussed above, the stripe phase is the ground state of the model (18) for $K > 0$. The spin-wave dispersion of the stripe phase was obtained previously in Refs. [13, 44, 45] and here we rederive the results to compare them latter with the orthomagnetic case. For concreteness, we first consider the stripe phase with ordering vector $\mathbf{Q}_1 = (\pi, 0)$. As shown in Fig.1(a), there are two spins per magnetic unit cell, whose HP operators we denote by $a_{\mathbf{k}}^{(1)}$ and $a_{\mathbf{k}}^{(2)}$. Note that, with respect to the spin coordinate system defined on site 1, the spin on site 2 is rotated by 180° , yielding:

$$\mathbf{S}^{(2)} = \left(-S_x^{(2)}, S_y^{(2)}, -S_z^{(2)} \right)_{(1)} \quad (25)$$

Using the Holstein-Primakoff transformation defined in Eq. 21, we find that the large- S Hamiltonian is given by:

$$\hat{\mathcal{H}}_{\mathbf{k}} = \begin{pmatrix} \epsilon_{\mathbf{k}} & 0 & 0 & \Delta_{\mathbf{k}} \\ 0 & \epsilon_{\mathbf{k}} & \Delta_{\mathbf{k}} & 0 \\ 0 & \Delta_{\mathbf{k}} & \epsilon_{\mathbf{k}} & 0 \\ \Delta_{\mathbf{k}} & 0 & 0 & \epsilon_{\mathbf{k}} \end{pmatrix} \quad (26)$$

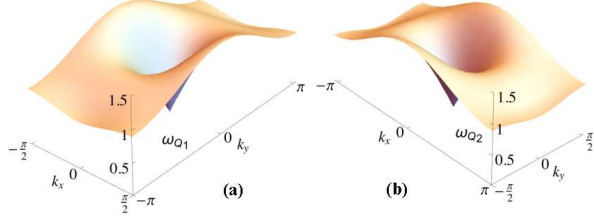


Figure 4: Spin-wave dispersions for the stripe phase with ordering vector $\mathbf{Q}_1 = (\pi, 0)$ (a) and $\mathbf{Q}_2 = (0, \pi)$ (b). Both are doubly degenerate Goldstone modes. The energies are in units of $4J_2S$. The parameters used are $J_1 = 0.8J_2$ and $K = 0.1J_2$.

with:

$$\begin{aligned} \epsilon_{\mathbf{k}} &= 2S [(J_1 - 2K) \cos k_y + 2J_2 + 4K] \\ \Delta_{\mathbf{k}} &= -2S (J_1 + 2K + 2J_2 \cos k_y) \cos k_x \end{aligned} \quad (27)$$

The Hamiltonian is diagonalized via the Bogoliubov transformation

$$\hat{\mathcal{U}}_{\mathbf{k}} = \begin{pmatrix} u_{\mathbf{k}} & 0 & 0 & v_{\mathbf{k}} \\ 0 & u_{\mathbf{k}} & v_{\mathbf{k}} & 0 \\ 0 & v_{\mathbf{k}} & u_{\mathbf{k}} & 0 \\ v_{\mathbf{k}} & 0 & 0 & u_{\mathbf{k}} \end{pmatrix} \quad (28)$$

with:

$$u_{\mathbf{k}}^2 = \frac{1}{2} \left(1 + \frac{\epsilon_{\mathbf{k}}}{\omega_{\mathbf{k}}} \right); \quad v_{\mathbf{k}}^2 = \frac{1}{2} \left(-1 + \frac{\epsilon_{\mathbf{k}}}{\omega_{\mathbf{k}}} \right); \quad u_{\mathbf{k}}v_{\mathbf{k}} = -\frac{1}{2} \frac{\Delta_{\mathbf{k}}}{\omega_{\mathbf{k}}} \quad (29)$$

yielding the doubly-degenerate eigenmode of the bosonic system:

$$\omega_{\mathbf{k}} = \sqrt{\epsilon_{\mathbf{k}}^2 - \Delta_{\mathbf{k}}^2} \quad (30)$$

Expanding near $k = 0$ gives (in polar coordinates):

$$\omega_{\mathbf{k}} \approx 4S |\mathbf{k}| \sqrt{\left(J_2 + K + \frac{J_1}{2} \right) \left(J_2 + K + \frac{J_1}{2} \cos 2\theta \right)} \quad (31)$$

showing that this eigenmode is indeed a Goldstone mode. The spin-wave dispersion for the stripe phase with ordering vector $\mathbf{Q}_2 = (0, \pi)$ can be calculated in the same way, yielding $\omega_{\mathbf{Q}_2}(k_x, k_y) = \omega_{\mathbf{Q}_1}(k_y, -k_x)$, as expected. In Fig. 4, we show the spin-wave mode (30) for the two types of stripe orders in their respective magnetic Brillouin zones. The results here are in agreement with those obtained previously elsewhere [13]. That we obtain doubly-degenerate Goldstone modes is a consequence of the fact that the ordered state is collinear and that $\omega_{\mathbf{k}+\mathbf{Q}_1} = \omega_{\mathbf{k}}$.

B. Orthomagnetic phase: spin-wave modes

The orthomagnetic phase becomes the ground state of Eq. (18) for $K < 0$. As shown in Fig.1(c), there are four spins per magnetic unit cell, giving rise to the HP operators $a_{\mathbf{k}}^{(1)}, a_{\mathbf{k}}^{(2)}, a_{\mathbf{k}}^{(3)},$ and $a_{\mathbf{k}}^{(4)}$. Because the spins on sites 2, 3, 4 correspond respectively to rotations of 90° , 180° , and 270° relative to the spin on site 1, we define the local spin coordinate systems:

$$\begin{aligned} \mathbf{S}^{(2)} &= (S_z^{(2)}, S_y^{(2)}, -S_x^{(2)})_{(1)} \\ \mathbf{S}^{(3)} &= (-S_z^{(3)}, S_y^{(3)}, S_x^{(3)})_{(1)} \\ \mathbf{S}^{(4)} &= (-S_x^{(4)}, S_y^{(4)}, -S_z^{(4)})_{(1)} \end{aligned} \quad (32)$$

Introducing $\Psi_{\mathbf{k}}^\dagger$ as defined in Eq. (21) and substituting in the Hamiltonian, we obtain in the large- S limit:

$$\hat{\mathcal{H}}_{\mathbf{k}} = \begin{pmatrix} \hat{A}_{\mathbf{k}} & \hat{B}_{\mathbf{k}} & \hat{C}_{\mathbf{k}} & \hat{D}_{\mathbf{k}} \\ \hat{B}_{\mathbf{k}} & \hat{A}_{\mathbf{k}} & \hat{D}_{\mathbf{k}} & \hat{C}_{\mathbf{k}} \\ \hat{C}_{\mathbf{k}} & \hat{D}_{\mathbf{k}} & \hat{A}_{\mathbf{k}} & \hat{B}_{\mathbf{k}} \\ \hat{D}_{\mathbf{k}} & \hat{C}_{\mathbf{k}} & \hat{B}_{\mathbf{k}} & \hat{A}_{\mathbf{k}} \end{pmatrix} \quad (33)$$

where we defined four 2×2 matrices, $\hat{A}_{\mathbf{k}}, \hat{B}_{\mathbf{k}}, \hat{C}_{\mathbf{k}},$ and $\hat{D}_{\mathbf{k}}$ of the form:

$$\hat{O}_{\mathbf{k}} = \begin{pmatrix} O_{1,\mathbf{k}} & O_{2,\mathbf{k}} \\ O_{2,\mathbf{k}} & O_{1,\mathbf{k}} \end{pmatrix} \quad (34)$$

with the matrix elements:

$$\begin{aligned} A_{1,\mathbf{k}} &= 4S(J_2 - K), \quad A_{2,\mathbf{k}} = -4SK \\ B_{1,\mathbf{k}} &= S(J_1 + 2K) \cos k_x, \quad B_{2,\mathbf{k}} = -S(J_1 - 2K) \cos k_x \\ C_{1,\mathbf{k}} &= S(J_1 + 2K) \cos k_y, \quad C_{2,\mathbf{k}} = -S(J_1 - 2K) \cos k_y \\ D_{1,\mathbf{k}} &= 0, \quad D_{2,\mathbf{k}} = -4SJ_2 \cos k_x \cos k_y \end{aligned} \quad (35)$$

The generalized Bogoliubov transformation is given by:

$$\hat{\mathcal{U}}_{\mathbf{k}} = \begin{pmatrix} \hat{X}_{\mathbf{k}} & \hat{Y}_{\mathbf{k}} & \hat{Z}_{\mathbf{k}} & \hat{W}_{\mathbf{k}} \\ \hat{X}_{\mathbf{k}} & -\hat{Y}_{\mathbf{k}} & \hat{Z}_{\mathbf{k}} & -\hat{W}_{\mathbf{k}} \\ \hat{X}_{\mathbf{k}} & \hat{Y}_{\mathbf{k}} & -\hat{Z}_{\mathbf{k}} & -\hat{W}_{\mathbf{k}} \\ \hat{X}_{\mathbf{k}} & -\hat{Y}_{\mathbf{k}} & -\hat{Z}_{\mathbf{k}} & \hat{W}_{\mathbf{k}} \end{pmatrix} \quad (36)$$

where the four 2×2 matrices, $\hat{X}_{\mathbf{k}}, \hat{Y}_{\mathbf{k}}, \hat{Z}_{\mathbf{k}},$ and $\hat{W}_{\mathbf{k}}$ are also of the form (34). For $\hat{X}_{\mathbf{k}}$, the matrix elements are given by:

$$\begin{aligned} X_{1,\mathbf{k}}^2 &= \frac{1}{8} \left(1 + \frac{\epsilon_{\mathbf{k}}}{\omega_{\mathbf{k}}} \right) \\ X_{2,\mathbf{k}}^2 &= \frac{1}{8} \left(-1 + \frac{\epsilon_{\mathbf{k}}}{\omega_{\mathbf{k}}} \right) \\ X_{1,\mathbf{k}}X_{2,\mathbf{k}} &= -\frac{1}{8} \frac{\Delta_{\mathbf{k}}}{\omega_{\mathbf{k}}} \end{aligned} \quad (37)$$

with:

$$\begin{aligned}\epsilon_{\mathbf{k}} &= A_{1,\mathbf{k}} + B_{1,\mathbf{k}} + C_{1,\mathbf{k}} + D_{1,\mathbf{k}} \\ \Delta_{\mathbf{k}} &= A_{2,\mathbf{k}} + B_{2,\mathbf{k}} + C_{2,\mathbf{k}} + D_{2,\mathbf{k}}\end{aligned}\quad (38)$$

and the eigenmode:

$$\omega_{\mathbf{k}} = \sqrt{\epsilon_{\mathbf{k}}^2 - \Delta_{\mathbf{k}}^2} \quad (39)$$

For the other matrix elements, we find:

$$\begin{aligned}Y_{i,\mathbf{k}} &= X_{i,\mathbf{k}+\mathbf{Q}_1} \\ Z_{i,\mathbf{k}} &= X_{i,\mathbf{k}+\mathbf{Q}_2} \\ W_{i,\mathbf{k}} &= X_{i,\mathbf{k}+\mathbf{Q}_1+\mathbf{Q}_2}\end{aligned}\quad (40)$$

Therefore, there are four non-degenerate eigenvalues of the bosonic system:

$$\omega_{1\mathbf{k}} = \omega_{\mathbf{k}}; \quad \omega_{2\mathbf{k}} = \omega_{\mathbf{k}+\mathbf{Q}_1}; \quad \omega_{3\mathbf{k}} = \omega_{\mathbf{k}+\mathbf{Q}_2}; \quad \omega_{4\mathbf{k}} = \omega_{\mathbf{k}+\mathbf{Q}_1+\mathbf{Q}_2} \quad (41)$$

with $\omega_{\mathbf{k}}$ given in Eq. (39). These four eigenmodes are shifted with respect to each other by the ordering vectors of the orthomagnetic phase, corresponding to in-phase or out-of-phase combinations of the four HP bosons. Expansion around $k = 0$ gives, in polar coordinates (recall that $K < 0$):

$$\begin{aligned}\omega_{1,\mathbf{k}} &\approx 4S |\mathbf{k}| \sqrt{\left(J_2 + \frac{J_1}{2}\right) (J_2 - K)} \\ \omega_{2,\mathbf{k}} &\approx 4S |\mathbf{k}| \sqrt{(J_2 - K) \left(J_2 + \frac{J_1}{2} \cos 2\theta\right)} \\ \omega_{3,\mathbf{k}} &\approx 4S |\mathbf{k}| \sqrt{(J_2 - K) \left(J_2 - \frac{J_1}{2} \cos 2\theta\right)} \\ \omega_{4,\mathbf{k}} &\approx 8S \sqrt{-2 \left(J_2 - \frac{J_1}{2}\right) K}\end{aligned}\quad (42)$$

Thus, of these four modes, three are Goldstone modes ($\omega_1, \omega_2, \omega_3$) and one (ω_4) is a gapped mode. All of them are shown in Fig. 5. Note also that while ω_1 is isotropic in the (k_x, k_y) plane, ω_2 and ω_3 are anisotropic and related by a 90° rotation. The fact that there are three spin-wave modes is a consequence of the non-collinear magnetic configuration of the orthomagnetic phase, which breaks completely all the spin-rotational symmetries of the system.

C. Dynamic structure factors of the stripe and orthomagnetic phases

Having established the nature of the spin-wave modes in the stripe and orthomagnetic phases, we now proceed

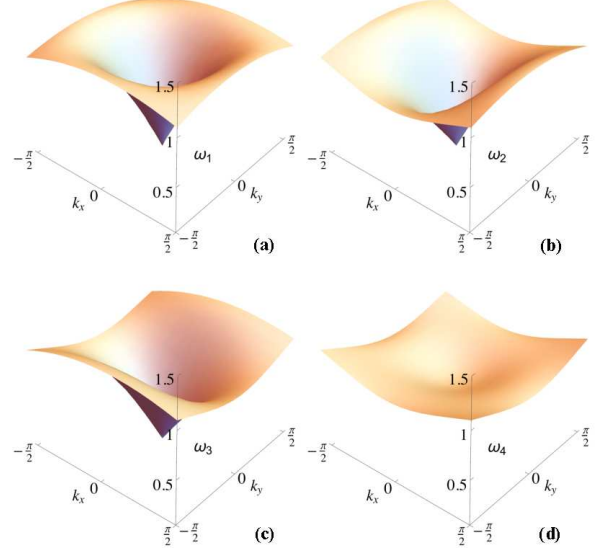


Figure 5: The eigenmodes of the non-collinear orthomagnetic order in the magnetic Brillouin zone. There are three Goldstone modes ($\omega_1, \omega_2, \omega_3$) and one gapped mode (ω_4). The four modes are linked by a shift of the momentum coordinate system by the orthomagnetic ordering vectors. Here, the energies are in units of $4J_2S$ and the parameters are $J_1 = 0.8J_2$ and $K = -0.1J_2$.

to compute the spin-spin correlation function $S_{\mu\nu}$, which can be measured by neutron scattering. We have [42, 43]:

$$S_{\mu\nu}(\mathbf{k}, \omega) = \int_{-\infty}^{\infty} \frac{dt}{2\pi} e^{-i\omega t} \langle S_{\mathbf{k}}^{\mu}(0) S_{-\mathbf{k}}^{\nu}(t) \rangle \quad (43)$$

where $\mu\nu = x, y, z$ refer to the spin components and $\mathbf{S}_{\mathbf{k}} \equiv \sum_r \mathbf{S}_{r,\mathbf{k}}$ is the sum over all the r spins in the magnetic unit cell. Here, the spin coordinate system is defined globally with respect to the neutron polarization, in contrast to the local coordinate system introduced in the previous subsection. For concreteness, hereafter we assume the incoming neutron to be polarized parallel to the spin on site 1, i.e. parallel to the \hat{z} axis. Computation of Eq. (43) is straightforward with the aid of the HP bosons and the Bogoliubov transformation defined in the previous subsection. Denoting by $\tilde{a}_{\mathbf{k}}^{(r)}$ the Bogoliubov-transformed bosonic operators, the only non-zero terms, at $T = 0$, are those of the form:

$$\int_{-\infty}^{\infty} \frac{dt}{2\pi} e^{-i\omega t} \langle \tilde{a}_{\mathbf{k}}^{(r)}(0) \tilde{a}_{\mathbf{k}}^{\dagger(r)}(t) \rangle = \delta(\omega - \omega_{r,\mathbf{k}}) \quad (44)$$

We first consider the stripe phase with the two possible ordering vectors $\mathbf{Q}_1 = (\pi, 0)$ and $\mathbf{Q}_2 = (0, \pi)$. We find that only the transverse components $S_{xx} = S_{yy}$ are non-zero, i.e. the longitudinal component S_{zz} and the off-diagonal components $S_{i \neq j}$ do not acquire spin-wave contributions. We obtain:

$$\mathcal{S}_{xx}^{\mathbf{Q}_i}(\mathbf{k}, \omega) = 2S(u_{\mathbf{k}} - v_{\mathbf{k}})^2 \delta(\omega - \omega_{\mathbf{k}}^{\mathbf{Q}_i}) \quad (45)$$

where $u_{\mathbf{k}}, v_{\mathbf{k}}$ are given by Eq. (29) and $\omega_{(k_x, k_y)}^{\mathbf{Q}_2} = \omega_{(-k_y, k_x)}^{\mathbf{Q}_1}$, with $\omega_{\mathbf{k}}^{\mathbf{Q}_1}$ given by Eq. (30). The total spin-spin correlation function, $\mathcal{S} = \sum_i \mathcal{S}_{ii}$ is then simply $\mathcal{S}(\mathbf{k}, \omega) = 2\mathcal{S}_{xx}(\mathbf{k}, \omega)$. In Fig. 6, we plot $\mathcal{S}(\mathbf{k}, \omega)$ for both the \mathbf{Q}_1 and \mathbf{Q}_2 stripe phases separately, as well as for a system containing equal domains of \mathbf{Q}_1 and \mathbf{Q}_2 :

$$\mathcal{S}_{\text{domain}}(\mathbf{k}, \omega) = \frac{1}{2}\mathcal{S}^{\mathbf{Q}_1}(\mathbf{k}, \omega) + \frac{1}{2}\mathcal{S}^{\mathbf{Q}_2}(\mathbf{k}, \omega) \quad (46)$$

The latter is the case relevant for the real systems, since twin domains are always formed in the iron pnictides. In all the plots, the delta function is replaced by a Lorentzian with width $\gamma = 0.05$ in units of $2J_2S$. From the figure, we see that the system with twin domains display symmetric spin-wave branches emerging from the ordering vectors $\mathbf{Q}_1 = (\pi, 0)$ and $\mathbf{Q}_2 = (0, \pi)$, as expected.

For the orthomagnetic phase, we find that all diagonal components \mathcal{S}_{ii} acquire spin-wave contributions. This is expected since the magnetic configuration is non-collinear (see Fig. 1), implying that all directions are “transverse” with respect to the sublattice 1 3 and/or the sublattice 2 4. In particular, we find:

$$\begin{aligned} \mathcal{S}_{xx}(\mathbf{k}, \omega) = \mathcal{S}_{zz}(\mathbf{k}, \omega) &= 4S(Y_{1,\mathbf{k}} + Y_{2,\mathbf{k}})^2 \delta(\omega - \omega_{2,\mathbf{k}}) \\ &\quad + 4S(Z_{1,\mathbf{k}} + Z_{2,\mathbf{k}})^2 \delta(\omega - \omega_{3,\mathbf{k}}) \\ \mathcal{S}_{yy}(\mathbf{k}, \omega) &= 16S(X_{1,\mathbf{k}} - X_{2,\mathbf{k}})^2 \delta(\omega - \omega_{1,\mathbf{k}}) \end{aligned} \quad (47)$$

with the Bogoliubov transformation parameters and spin-wave modes defined in Eqs. (37) and (41). In Fig. 7, we plot these diagonal components as well as the total structure factor $\mathcal{S} = \sum_i \mathcal{S}_{ii}$. In the latter, we observe two anisotropic spin-wave branches emerging from the ordering vectors $\mathbf{Q}_1 = (\pi, 0)$ and $\mathbf{Q}_2 = (0, \pi)$, in sharp contrast to the case of domains of stripes, where only one spin-wave branch emerges from each ordering vector (see Fig. 6). While the spin-wave velocities of the two branches are equal along the longitudinal direction (i.e. $\mathbf{k} \parallel \mathbf{Q}_i$), $c_{1,\text{long}} = c_{2,\text{long}}$, they become different along the transverse direction (i.e. $\mathbf{k} \perp \mathbf{Q}_i$):

$$\frac{c_{1,\text{transv}}}{c_{2,\text{transv}}} = \sqrt{\frac{2J_2 + J_1}{2J_2 - J_1}} \quad (48)$$

Interestingly, this ratio does not depend on the bi-quadratic coupling K . These qualitative features, in principle, allow one to experimentally distinguish, in an unambiguous way, whether the magnetic ground state is stripe or orthomagnetic. Note that, in the orthomagnetic phase, no spin-wave modes emerge from $\mathbf{Q}_1 + \mathbf{Q}_2 = (\pi, \pi)$.

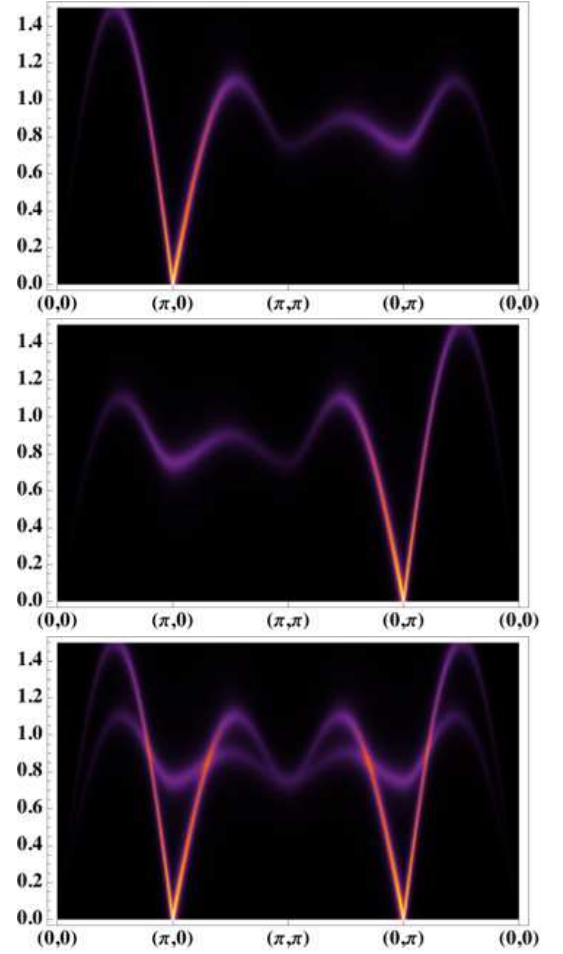


Figure 6: The total spin-spin structure factor $\mathcal{S} = \sum_i \mathcal{S}_{ii} = 2\mathcal{S}_{xx}$ for the \mathbf{Q}_1 (top panel) and \mathbf{Q}_2 (mid panel) stripe phases. Bottom panel is the structure factor assuming equal domains of \mathbf{Q}_1 and \mathbf{Q}_2 stripes. The vertical axis is the energy measured in units of $4J_2S$, whereas the horizontal axis displays intensity cuts in the Fe-square-lattice Brillouin zone. The intensity is highest at the ordering vectors \mathbf{Q}_1 and \mathbf{Q}_2 . The parameters used here are $J_1 = 0.8J_2$ and $K = 0.1J_2$.

Continuing the investigation of the orthomagnetic phase, we find that the spin-waves also contribute to the off-diagonal component:

$$\begin{aligned} \mathcal{S}_{xz}(\mathbf{k}, \omega) &= 4S(Y_{1,\mathbf{k}} + Y_{2,\mathbf{k}})^2 \delta(\omega - \omega_{2,\mathbf{k}}) \\ &\quad - 4S(Z_{1,\mathbf{k}} + Z_{2,\mathbf{k}})^2 \delta(\omega - \omega_{3,\mathbf{k}}) \end{aligned} \quad (49)$$

providing another criterion to distinguish experimentally the orthomagnetic and stripe phases. In principle, the structure factor tensor of the orthomagnetic phase can be brought in a diagonal form if the neutron is polarized along $\tilde{\mathbf{z}} = (\mathbf{x} + \mathbf{z})/\sqrt{2}$. In this new coordinate system, each of the three Goldstone modes contribute only to one of the diagonal components, and we find:

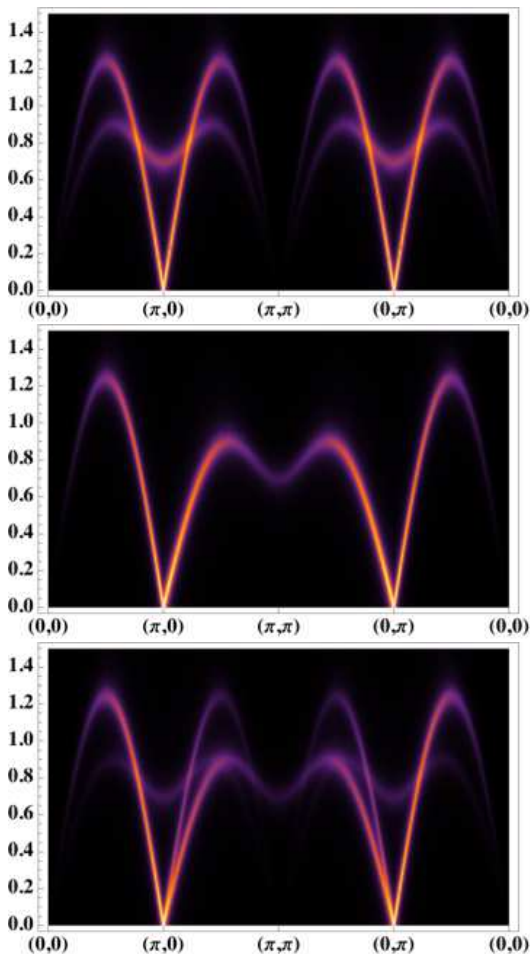


Figure 7: The structure factors $\mathcal{S}_{xx} = \mathcal{S}_{zz}$ (top panel), \mathcal{S}_{yy} (mid panel) and $\mathcal{S} = \sum_i \mathcal{S}_{ii}$ (bottom panel) for the orthomagnetic phase. The vertical axis is the energy measured in units of $4J_2S$, whereas the horizontal axis displays momentum cuts in the Fe-square-lattice Brillouin zone. The parameters used here are $J_1 = 0.8J_2$ and $K = -0.1J_2$. Two anisotropic spin-wave branches emerge from the ordering vectors $\mathbf{Q}_1 = (\pi, 0)$ and $\mathbf{Q}_2 = (0, \pi)$, in sharp contrast to the case of domains of stripes shown in Fig. 6.

$$\begin{aligned}\tilde{\mathcal{S}}_{zz}(\mathbf{k}, \omega) &= 8S(Y_{1,\mathbf{k}} + Y_{2,\mathbf{k}})^2 \delta(\omega - \omega_{2,\mathbf{k}}) \\ \tilde{\mathcal{S}}_{xx}(\mathbf{k}, \omega) &= 8S(Z_{1,\mathbf{k}} + Z_{2,\mathbf{k}})^2 \delta(\omega - \omega_{3,\mathbf{k}})\end{aligned}\quad (50)$$

as well as $\tilde{\mathcal{S}}_{yy} = \mathcal{S}_{yy}$.

IV. DISCUSSION AND CONCLUSIONS

We investigated in details under what conditions the orthomagnetic state, which displays a non-collinear double- \mathbf{Q} tetragonal magnetic structure, becomes the magnetic ground state of the iron pnictides within a microscopic itinerant model. We found that large deviations from perfect nesting favor a tetragonal magnetic

state, but do not select between the non-collinear and non-uniform configurations – Figs. 1(c) and (d), respectively. Instead, the non-collinear order is favored by the residual electronic interactions that do not participate in the SDW – in agreement with the results found in Ref. [22] – whereas the non-uniform state is favored by coupling to soft Neel-like fluctuations, as discussed by two of us in Ref. [21]. Our investigation is complementary to previous works reporting that different regions of the large parameters space of the iron-based superconductors may display magnetic ground states that do not break tetragonal symmetry [21–24]. In particular, Ref. [18] showed that the same three-band model studied in Section II accounts for a transition inside the magnetic stripe state to the C_4 -magnetic state. Our findings reveal that the tetragonal magnetic state can also appear as the primary magnetic instability of the system, without requiring pre-existing stripe order.

The significance of the observation of tetragonal magnetic states in $\text{Ba}(\text{Fe}_{1-x}\text{Mn}_x)_2\text{As}_2$, $(\text{Ba}_{1-x}\text{K}_x)\text{Fe}_2\text{As}_2$, and $(\text{Ba}_{1-x}\text{Na}_x)\text{Fe}_2\text{As}_2$ relies on its implication to the nature of the magnetism of these materials. First, the existence of magnetic Bragg peaks at $\mathbf{Q}_1 = (\pi, 0)$ and $\mathbf{Q}_2 = (0, \pi)$ in the absence of a splitting of the lattice Bragg peaks implies that the tetragonal symmetry-breaking is not a prerequisite for the formation of magnetic order, challenging the point of view that ferro-orbital order is the leading normal-state instability. Furthermore, because the non-collinear and non-uniform magnetic states do not belong to the ground state manifold of the J_1 - J_2 model, the latter is likely not the most suitable low-energy model to describe the magnetic properties of the iron-based superconductors.

Of course, these statements rely on the confirmation that $\text{Ba}(\text{Fe}_{1-x}\text{Mn}_x)_2\text{As}_2$, $(\text{Ba}_{1-x}\text{K}_x)\text{Fe}_2\text{As}_2$, and $(\text{Ba}_{1-x}\text{Na}_x)\text{Fe}_2\text{As}_2$ do display tetragonal magnetic order. Up to now, the observations have focused on the absence of detectable structural distortion, which is usually large in most iron-based materials [17] due to their sizable magneto-elastic coupling [46]. Nevertheless, given the resolution limitations intrinsic to x-ray and neutron diffraction probes [32], it is desirable to find other signatures of these tetragonal magnetic states. Here, we have shown how qualitative features in the spin-wave spectrum can unambiguously distinguish between the stripe and orthomagnetic (non-collinear) phases. For instance, while the latter displays two anisotropic spin-wave branches emerging from each of the ordering vectors $\mathbf{Q}_1 = (\pi, 0)$ and $\mathbf{Q}_2 = (0, \pi)$, a system with domains of the two distinct stripe states displays a single spin-wave branch emerging from each of them. Furthermore, only in the orthomagnetic phase the spin waves can also be detected in off-diagonal components of the spin-spin correlation function. These two distinguishing features can in principle be probed by unpolarized and polarized neutron scattering experiments, respectively. We have not discussed the spin-wave spectrum of the non-collinear phase, which is beyond the scope of the current paper. Yet,

because this state is collinear, one does not expect the appearance of additional Goldstone modes, as in the orthomagnetic phase. Interesting features can appear at the ordering vector $\mathbf{Q}_1 + \mathbf{Q}_2 = (\pi, \pi)$ in the non-collinear phase due to the formation of a composite order parameter, as discussed in Ref. [21]. It remains to be seen how these tetragonal magnetic states affect the superconducting state.

Finally, we note that the results obtained here for the spin-wave spectra of the stripe and orthomagnetic phases can also be useful to determine the magnetic states of other compounds that display magnetic Bragg peaks at $\mathbf{Q}_1 = (\pi, 0)$ and $\mathbf{Q}_2 = (0, \pi)$ but no orthorhombic distortion. In general, without knowledge of the size of the magneto-elastic coupling, it is difficult to establish whether these observations are consistent with domains of stripes or orthomagnetic order. A recent example is the compound GdRhIn₅, which is related to the 115 family of heavy fermions [34]. Although resonant x-ray scattering found evidence for magnetic order at momenta \mathbf{Q}_1 and \mathbf{Q}_2 , synchrotron x-rays were unable to resolve a structural distortion. Furthermore, the magnetic transition seems to be second-order, which is difficult to reconcile with a simultaneous structural transition. An interesting alternative would be the formation of an orthomagnetic state, which could be identified by neutron scattering experiments deep inside the magnetically ordered state.

V. ACKNOWLEDGEMENTS

We thank A. Böhrer, P. Canfield, M. Chan, A. Chubukov, I. Eremin, A. Goldman, M. Greven, C. Meingast, R. McQueeney, R. Osborn, P. Pagliuso, L. Taillefer, and G. Yu for fruitful discussions. This work was supported by the Department of Energy under Award Number DE-SC0012336.

Appendix A: Contribution of the residual interactions to the free energy

Here we show how to explicitly compute the contribution of the residual interactions $U_2, U_4, U_5, U_6, U_7,$ and U_8 in Eq. (3) to the free energy. We illustrate the procedure by considering the U_7 term, corresponding to an exchange-like interaction between the electron pockets

at \mathbf{Q}_1 and \mathbf{Q}_2 . To lowest order in U_7 , the contribution to the free energy corresponds to the two Feynman diagrams shown in Fig. 3 in the main text. Because we are interested in the uniform limit of the action, the momentum of the fields \mathbf{M}_1 and \mathbf{M}_2 is set to zero. Also, because we are approaching the transition from the paramagnetic side, we ignore the corrections to the electronic Green's functions due to the presence of SDW order.

Denoting the generalized momentum by q , the left diagram corresponds to

$$U_7 \left(M_1^i M_2^l M_2^j M_1^k \right) \left(\sigma_{\alpha\mu}^i \sigma_{\mu\alpha}^l \sigma_{\beta\nu}^j \sigma_{\nu\beta}^k \right) [G_h(q) G_{e_1}(q) G_{e_2}(q) G_h(p) G_{e_1}(p) G_{e_2}(p)] \quad (\text{A1})$$

where i, j, k, l correspond to vector components and repeated index are implicitly summed. The sum over Pauli matrices is equivalent to:

$$\text{Tr} \{ \sigma^i \sigma^l \} \text{Tr} \{ \sigma^j \sigma^k \} = 4 \delta^{il} \delta^{jk} \quad (\text{A2})$$

As a result, this diagram gives the contribution

$$4U_7 \left(\sum G_h G_{e_1} G_{e_2} \right)^2 (\mathbf{M}_1 \cdot \mathbf{M}_2)^2 \quad (\text{A3})$$

The right diagram corresponds to:

$$-U_7 \left(M_1^i M_2^l M_2^j M_1^k \right) \left(\sigma_{\mu\beta}^i \sigma_{\beta\nu}^l \sigma_{\nu\alpha}^j \sigma_{\alpha\mu}^k \right) [G_h(q) G_{e_1}(q) G_{e_2}(q) G_h(p) G_{e_1}(p) G_{e_2}(p)] \quad (\text{A4})$$

where the minus sign comes from the closed fermionic loop. Using the identity:

$$\text{Tr} \{ \sigma^i \sigma^l \sigma^j \sigma^k \} = 2(\delta^{il} \delta^{jk} - \delta^{ij} \delta^{kl} + \delta^{ik} \delta^{jl}) \quad (\text{A5})$$

we obtain:

$$\begin{aligned} & -2U_7 \left(\sum G_h G_{e_1} G_{e_2} \right)^2 M_1^2 M_2^2 \\ & = -\frac{U_7}{2} \left(\sum G_h G_{e_1} G_{e_2} \right)^2 \left[(\mathbf{M}_1^2 + \mathbf{M}_2^2)^2 - (\mathbf{M}_1^2 - \mathbf{M}_2^2)^2 \right] \end{aligned} \quad (\text{A6})$$

All the other terms can be computed in an analogous way.

[1] Y. Kamihara, T. Watanabe, M. Hirano and H. Hosono, *J. Am. Chem. Soc.* **130**, 3296 (2008).
 [2] K. Ishida, Y. Nakai and H. Hosono, *J. Phys. Soc. Japan* **78**, 062001 (2009); D. C. Johnston, *Adv. Phys.* **59**, 803 (2010); J. Paglione and R. L. Greene, *Nature Phys.* **6**, 645 (2010); P. C. Canfield and S. L. Bud'ko, *Annu. Rev. Cond. Mat. Phys.* **1**, 27 (2010); H. H. Wen and S. Li,

Annu. Rev. Cond. Mat. Phys. **2**, 121 (2011).
 [3] Xingye Lu *et al*, *Science* **345**, 657(2014).
 [4] E. C. Blomberg, M. A. Tanatar, A. Kreyssig, N. Ni, A. Thaler, Rongwei Hu, S. L. Bud'ko, P. C. Canfield, A. I. Goldman, and R. Prozorov, *Phys. Rev. B* **83**, 134505 (2011).
 [5] R. M. Fernandes, A. V. Chubukov, and J. Schmalian,

- Nature Phys. **10**, 97 (2014).
- [6] P. Dai, J. Hu, and E. Dagotto, Nature Phys. **8**, 709 (2012).
- [7] I. Eremin, J. Knolle, R. M. Fernandes, J. Schmalian, and A. V. Chubukov, J. Phys. Soc. Jpn. **83**, 061015 (2014).
- [8] M. D. Johannes and I. I. Mazin, Phys. Rev. B **79**, 220510(R) (2009).
- [9] W. Z. Hu *et al.*, Phys. Rev. Lett. **101**, 257005 (2008)
- [10] W.C. Lv, J. Wu and P. Phillips, Phys. Rev. B **80**, 224506 (2009)
- [11] C. C. Lee, W. G. Yin, and W. Ku, Phys. Rev. Lett. **103**, 267001 (2009).
- [12] R. Applegate, R. R. P. Singh, C.-C. Chen, and T. P. Devereaux, Phys. Rev. B **85**, 054411 (2012).
- [13] C. Fang, H. Yao, W.-F. Tsai, J. P. Hu and S. A. Kivelson, Phys. Rev. B **77**, 224509 (2008)
- [14] C. Xu, M. Muller, and S. Sachdev, Phys. Rev. B **78**, 020501(R) (2008).
- [15] R. M. Fernandes, A. V. Chubukov, J. Knolle, I. Eremin and J. Schmalian, Phys. Rev. B **85**, 024534 (2012)
- [16] S. Liang, A. Mukherjee, N. D. Patel, E. Dagotto, and A. Moreo, arXiv:1405.6395
- [17] M. G. Kim *et al.*, Phys. Rev. B **82**, 220503(R) (2010)
- [18] S. Avcı *et al.*, Nature Comm. **5**, 3845 (2014)
- [19] A. Böhmer and C. Meingast, private communication.
- [20] E. Hassinger, G. Gredat, F. Valade, S. Rene de Cotret, A. Juneau-Fecteau, J.-Ph. Reid, H. Kim, M. A. Tanatar, R. Prozorov, B. Shen, H.-H. Wen, N. Doiron-Leyraud, and L. Taillefer, Phys. Rev. B **86**, 140502 (2012).
- [21] X. Wang and R. M. Fernandes, Phys. Rev. B **89**, 144502 (2014)
- [22] I. Eremin and A. V. Chubukov, Phys. Rev. B **81**, 024511 (2010).
- [23] J. Lorenzana, G. Seibold, C. Ortix, and M. Grilli, Phys. Rev. Lett. **101**, 186402 (2008).
- [24] P. M. R. Brydon, J. Schmiedt, and C. Timm, Phys. Rev. B **84**, 214510 (2011).
- [25] B. Barbara, M. F. Rossignol, J. X. Boucherle, and C. Vettier, Phys. Rev. Lett. **45**, 938 (1980).
- [26] A Stunault *et al.*, J. Phys.: Condens. Matter **21**, 376004 (2009).
- [27] J. Jensen and M. Rotter, Phys. Rev. B **77**, 134408 (2008).
- [28] P. S. Normile, M. Rotter, C. Detlefs, J. Jensen, P. C. Canfield, and J. A. Blanco, Phys. Rev. B **88**, 054413 (2013).
- [29] J. Jensen and P. Bak, Phys. Rev. B **23**, 6180(R) (1981).
- [30] R. S. Fishman and S. H. Liu, Phys. Rev. B **59**, 8681 (1999).
- [31] P. Chandra, P. Coleman and A. I. Larkin, Phys. Rev. Lett. **64**, 88-91 (1990)
- [32] D. S. Inosov *et al.*, Phys. Rev. B **87**, 224425 (2013).
- [33] D. D. Khalyavin, S. W. Lovesey, P. Manuel, F. Kruger, S. Rosenkranz, J. M. Allred, O. Chmaissem, and R. Osborn, arXiv:1409.5324.
- [34] E. Granado *et al.*, Phys. Rev. B **74**, 214428 (2006)
- [35] A. V. Chubukov, D. V. Efremov and I. Eremin, Phys. Rev. B **78**, 134512 (2008)
- [36] S. Maiti and A. V. Chubukov, Phys. Rev. B **82**, 214515 (2010)
- [37] R. Thomale, C. Platt, J. Hu, C. Honerkamp, and B. A. Bernevig, Phys. Rev. B **80**, 180505(R) (2009).
- [38] E. Berg, S. A. Kivelson, and D. J. Scalapino, Phys. Rev. B **81**, 172504 (2010).
- [39] M. W. Long and W. Yeung, J. Phys. F: Met. Phys. **17**, 1175 (1987).
- [40] Y. Kamiya, N. Kawashima, and C. D. Batista, Phys. Rev. B **84**, 214429 (2011).
- [41] A. Chubukov, E. Gagliano, and C. Balseiro, Phys. Rev. B **45**, 7889 (1992).
- [42] E. W. Carlson, D. X. Yao, and D. K. Campbell, Phys. Rev. B **70**, 064505 (2004).
- [43] J. T. Haraldsen and R. S. Fishman, J. Phys.: Condens. Matter **21** (2009) 216001
- [44] D. X. Yao and E. W. Carlson, Phys. Rev. B **78**, 052507 (2008).
- [45] R. Applegate, J. Oitmaa, and R. R. P. Singh, Phys. Rev. B **81**, 024505 (2010).
- [46] A. Patz, T. Li, S. Ran, R. M. Fernandes, J. Schmalian, S. L. Bud'ko, P. C. Canfield, I. E. Perakis, and J. Wang, Nature Comm. **5**, 3229 (2014).